A Method of Forming Composite Structures Using *In Situ*-Formed Liquid Crystal Polymer Fibers in a Thermoplastic Matrix

B. R. BASSETT *and* A. F. YEE*

Departments of Materials Science and Engineering and Macromolecular Science and Engineering
University of Michigan
Ann Arbor, Michigan 48109

A new high speed and potentially economical method of creating a composite material and structures therefrom is tested. The method consists of spinning composite fibers from a melt blend of a thermoplastic with a liquid crystal polymer (LCP). Discontinuous fibrils of the LCP are formed *in situ* during the spinning process. These composite fibers are aligned and placed in a mold and heated to melt the thermoplastic matrix, but not the fibrils. A finished composite structure reinforced by the LCP fibrils is obtained when the thermoplastic phase is consequently consolidated. Our experiments show the proposed process is reasonable for an easily processed polystyrene matrix. High modulus fibrils with essentially infinite L/D ratios are readily produced in the extrusion process using 40 wt% of a wholly aromatic poly(ester-co-amide) LCP from Celanese. The integrity and alignment of the LCP fibrils is retained in the molding step. Mechanical tests show that the fibers produced by high shear rate processing have a stiffness approaching 23 GPa and match an axial rule-of-mixtures theory. The use of polystyrene resulted in brittleness. Molded composite plates exhibit slightly lower stiffness and significantly lower strength than individual fibers.

INTRODUCTION

This paper describes experiments performed in an effort to learn the feasibility of producing composite structures by an unusual and potentially low cost method. *Figure 1* shows schematically the steps involved in reaching the finished composite structure. In the first step, a liquid crystal polymer (LCP) and a thermoplastic are blended and spun into a fiber with dispersed fibrils of LCP in a thermoplastic matrix. The cross-sectional view in *Fig. 1* shows the desired fiber morphology with reinforcement provided by the axially aligned dispersed fibrils. The second step consists of forming a cloth or unidirectional tow of fibers. Finally, in the third step, the cloth is heated in a mold to melt and consolidate the thermoplastic matrix. Molding temperature is chosen to melt the thermoplastic without melting the LCP fibrils. Fibril reinforcement is thereby retained in the finished composite structure.

The proposed material has several potential advantages over current thermoplastic composites:

- The woven cloth could conform to mold configurations that a 'prepreg' thermoplastic sheet composite cannot.
- The two components are intimately mixed. Provided that the interfacial energy is favorable, fiber wetting problems are inherently removed. In addition, matrix viscosity is no longer limited by flow and wetting considerations—creating the potential for using a high viscosity matrix material.
- The material is 100% recycleable. Material to be recycled may be chopped up, melted, and respun to recreate the aligned fibril reinforced composite.
- Potential low processing cost. There is only one operation involved in creating both the reinforcing fiber and matrix, and that operation can be per-

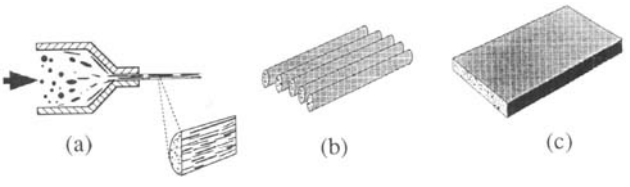

Fig. 1. (a) A liquid blend consisting of a thermoplastic with dispersed liquid crystal polymer (LCP) droplets is passed through a capillary die to produce a fiber reinforced by dispersed LCP fibrils. A cross sectional view of the fiber is also shown. (b) Fibers are arranged in a tow or cloth. (c) Tow is molded to melt and consolidate thermoplastic matrix without altering LCP fibrils. Resulting is a fiber reinforced thermoplastic composite structure.

* To whom correspondence should be addressed.

formed on convention polymer processing equipment.

There are, unfortunately, also problems with this idea. One of the largest constraints is the inherent fiber loading limit—our experiments show that about 40 wt% (34 vol%) LCP marks the upper limit of discrete fibril formation for the particular blend and conditions in our experiments.

Our experimental objective has been to investigate the feasibility of producing composite structures by the proposed method. This paper presents the results of that investigation.

Background

The production of traditional fiber composites begin by making the reinforcing fibers. These fibers are sized and woven into a cloth or gathered into a tow. To form the composite, a matrix resin is made to flow through the cloth and wet the individual fibers. To be able to do so, the matrix must possess low viscosity. Unfortunately, in the case of thermoplastic composites, lowered viscosity often correlates to reduced mechanical performance.

Polymeric fibers are produced by well-known spinning methods. These methods involve varying degrees of complexity. In the case of Du Pont's aramid fiber, Kevlar, the processing requires sulfuric acid solution spinning because the molecules are otherwise intractable. Some organic fibers can be formed by an entirely different and potentially far simpler process: *in-situ* fiber formation. This process involves producing a molten mixture of two immiscible polymers with one polymer forming droplets in a matrix of the second polymer. These droplets are deformed by flow of the mixture. Elongation forces cause the droplets to stretch into elliptical shapes and further into fibrils. The theory of droplet deformation has been developed by Taylor (1) and expanded by others (2, 3). Van Oene developed a theory that predicts conditions necessary for fibril formation (4). Tsebrenko, *et al.* have performed extensive studies on fibril formation using poly(oxymethylene) in various matrices (5, 6).

Thermotropic liquid crystal polymers exhibit properties that make them quite attractive as potential dispersed phase *in-situ* reinforcing materials. Thermotropic LCP's are essentially rigid-rod long-chain molecules with some irregularity or flexibility incorporated into the polymer chain to lower the melting point below the decomposition temperature. The rigid-rod molecular structure allows these materials to exhibit molecular order in a liquid mesophase. This ordering can lead to highly anisotropic mechanical properties with superior stiffness and strength in the direction of molecular alignment. When utilized for *in-situ* reinforcement, the LCP may be expected to yield substantial reinforcement as a result of these exceptional mechanical properties.

Recent papers describe the mechanical properties of injection molded blends utilizing a liquid crystal polymer added to a thermoplastic (7, 8). The LCP can substantially increase the mechanical performance of the injection-molded specimen. Yet injection molding involves extremely complex flow patterns which necessarily leads to variations in orientation of the LCP phase. For example, in thin sections taken from varying depths through injection molded specimens, Kiss reported seven distinct morphologies (8). Because of this variable orientation, the mechanical properties of uniformly oriented LCP specimens are not attained in injection molding.

Extrusion involves less complex flow patterns than injection molding. Blizard and Baird (9, 10) have examined the morphology of extruded rods of LCP/polycarbonate (PC) and LCP/nylon 6,6 blends. Rods were quenched immediately after exiting the extruder. At a ratio of 30 w/0 (wt%) LCP in PC, well developed fibrils were observed. Mechanical testing showed significant improvement in stiffness and strength with the addition of LCP.

Processing experiments using pure LCP show that if the extrudate is drawn after extrusion large increases in molecular alignment and mechanical properties are observed (11, 12). The elongational stresses present in the drawing process are responsible for creating this alignment, while the shear stresses present in the capillary do little to produce alignment (13). This behavior also occurs in blends. Isayev and Modic blended polycarbonate (PC) with Celanese LCP-2000 and spun fibers from the extrudate of a capillary rheometer (14). At 10% LCP, well defined fibrils formed in the LCP phase, but higher weight fractions of LCP resulted in spherical LCP particles. Kiss examined extruded and drawn strands of Polyethersulfone (PES) with 30 w/0 LCP of varying chemical structures; LCP fibrils were clearly evident in morphological examinations. The exact processing conditions are not described, but significant modulus enhancement was observed as a result of LCP addition to the PES (8). Chung tested extruded blends of nylon 12 and a Celanese aromatic polyester LCP with a draw ratio between 4 and 7 (estimated from die and sizing ring diameters) (15). He observed fine LCP fibrils in the 20% LCP blend. Amano and Nakagawa studied extruded, drawn blends of poly(ethylene terephthalate) with 30% LCP and determined their sonic modulus as a function of draw ratio. Their results appear to contradict those for pure LCP's by showing that modulus improvement occurs as a result of the matrix PET modulus improvement rather than because the dispersed LCP phase is becoming stiffer (16).

Our research objective has been to produce fibers reinforced by *in-situ* formed fibrils which can then be molded into a thermoplastic composite structure retaining the fibril reinforcement.

EXPERIMENTAL

Material

The matrix component used was polystyrene (Dow XP6069.02 Polystyron) in the form of pellets. The molecular weights were Mw = 318,400 and Mn =

169,000 with a polydispersity index of 1.88. These values were obtained from gel permeation chromatography using toulene as the solvent.

The liquid crystal polymer used in these experiments was Celanese Vectra B-900 supplied in the form of extruded pellets. Celanese describes this as a wholly aromatic liquid crystal poly(ester-co-amide) with a molecular weight greater than 20,000. The detailed composition of this LCP was not disclosed by the manufacturer. Celanese reports the density of B-900 as 1.37–1.42 g/cc. The basic components of this material are pictured in *Fig. 2.* We estimate the average chain length at about 150 of these repeat units. The contour length of this molecule is estimated to be 130 nm. Both the polystyrene and LCP were analyzed using differential scanning calorimetry with a Perkin Elmer DSC 7 and a 10°C/min heating rate.

PS, LCP, and their blend were rheologically characterized using an Instron capillary rheometer model 3210. A 1″ by .03″ die (L/D = 33) was used. The data were adjusted using a Rabinowitz velocity profile correction. An entrance correction was not applied.

Fiber Processing

Polystyrene pellets were dried in a vacuum oven for 24 h at 90°C before processing. LCP pellets were dried in a vacuum oven for 24 hours at 150°C. Pellets were then weighed and mixed together in a jar which was tumbled until complete mixing was observed. The mixture was poured into the extruder hopper and a cover was placed over the hopper.

Preliminary experiments showed that discrete fibrils of LCP are formed at ratios of up to 40 wt% LCP (34 vol%). At 50 w/0 LCP the fibrils begin to form a continuous network rather than remaining discrete. The following experiments were performed with 40 w/0 LCP to maximize fibril loading while maintaining the discreteness of the fibrils.

The processing equipment is shown in *Fig. 3.* It consisted of the following components:

- Brown ¾″ extruder with feed zone temperature set to 93°C (200°F) and compression zone temperature set to 280°C (535°F).
- Ross ISG static mixer with six four-way mixing elements and a 2.54 cm (1″) diameter housing. Three heater bands and a controlling thermocouple were placed outside the housing. Insulation was wrapped over the entire unit. The temperature of the mixer was set at 280°C (535°F).
- Adaptor attached to the end of the mixer which allowed a capillary die to be placed at the exit from the mixer. This adaptor also held a Dynisco pressure transducer. The adaptor and die were wrapped with insulation.
- Instron capillary rheometer die with length 1″, diameter .03″ and L/D = 33.
- Brown drawing apparatus with variable speed take-up at speeds up to 1.52 m/s (5 ft/s). In this device, extruded fibers passed over two rollers and through a pair of drawing wheels. The distance between the die and the first wheel was ~2′. The extrudate was not quenched.

Flow rates were obtained by collecting the extrudates for fixed amounts of time and weighing. Shear rates were calculated using this information. Shear stresses were calculated from pressures observed ahead of the die.

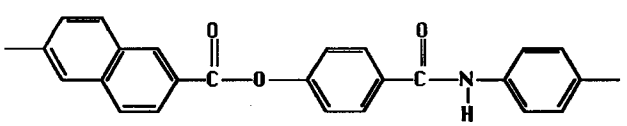

Fig. 2. Vectra B900 is described by Celanese as a wholly aromatic polyesteramide with naphthoic moities added to reduce polymer rigidity and hence lower melting point below chemical degradation temperature. One possible polymer structure is shown. The exact monomers and the proportion of each are proprietary.

Composite Processing

Molded specimens were formed in a 15.2 cm (6″) by 1.27 cm (½″) compression mold (see *Fig. 4*). Fibers were placed in the mold and held by clamping at the ends. The mold was then placed in a heated press (Preco model PA7) at 177°C (350°F) and light pressure was applied until the mold had reached 150°C. At that time the pressure was increased to 13.3 MPa (1670 psi) to consolidate the fibers. After the pressure was held for 30 sec. the heat was turned off and cooling water was run through the platens to quench the sample. The pressure dropped about 10% during the quench as the specimen contracted. When the temperature dropped to 93°C (200°F), the pressure was released and the mold was removed and opened.

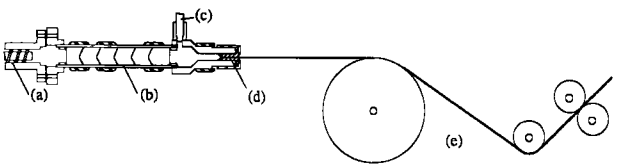

Fig. 3. Fiber processing equipment. (a) Brown ¾″ single screw extruder. (b) Ross 6 element, 1″ diameter static mixer. (c) Dynisco pressure transducer and thermocouple. (d) Instron capillary rheometer die. L = 1″, D = .0301″. (e) Drawing apparatus: Chill wheel and drawing wheels.

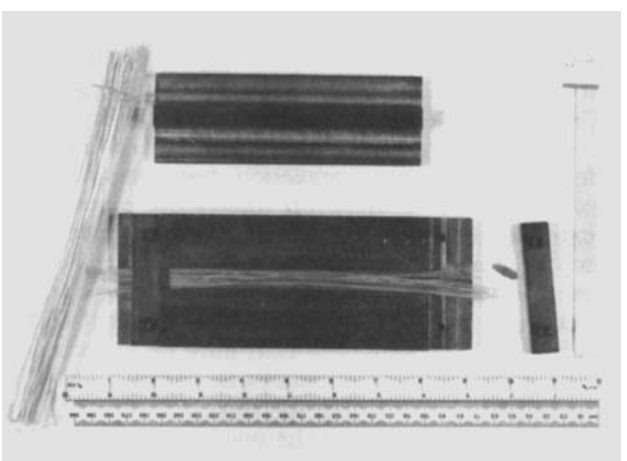

Fig. 4. Mold, fibers, and molded specimen.

Morphological and Mechanical Analysis

Fibril Morphology

Fibers were placed on glass microscope slides which were then eluted with toluene to dissolve the polystyrene matrix without altering the dispersed LCP phase. Tweezers were used to gently pull apart the fiber and spread out the fibrils. Samples were then dried, sputter coated, and viewed in a Hitachi model S-520 scanning electron microscope (SEM).

Fracture Surface Examinations

Drawn fibers were fractured in tension at room temperature. Undrawn fibers were fractured in flexure at room temperature. Samples were then mounted, sputter coated, and examined in the SEM.

Thin sections were made on a Sorvall MT2-B ultramicrotome using glass knives. Section thicknesses were 0.5 to 3 μm. These samples were viewed on a Nikon Optiphot microscope.

Fibers were tested for longitudinal stiffness and strength in an Instron model TTB tensile tester. Specimens for modulus tests were held with serrated grips covered with sandpaper of fine grit. These fibers were aligned with the aid of a sheet of paper with a printed grid placed behind the grips. Specimens for strength tests were held using rubber pads on the serrated grips to reduce stress concentration. These fibers were aligned by mounting them first on strips of paper. After the strip of paper was mounted and aligned in the grips, it was cut, and then the test was performed. All mechanical tests were performed with a 10.2 cm (4") grip separation which was assumed to be the gage length. Tests were performed at a constant crosshead speed of .021 mm/s (.05" per minute). The nominal strain rate is therefore 1.25×10^{-2} min^{-1}. A 10-lb Instron load cell was used to measure the fiber load. Due to the brittleness of these fibers, many failed by fracture at the grips, and the strength data should be considered with this in mind. All data points represent the average of at least five tests.

Molded specimens were also tested in tension. A servo-hydraulic testing machine (Instron model 1332) was used for these experiments with a 1000 lb load cell set to the most appropriate range for the predicted load at fracture. Cross head speed was .127 mm/s (0.3 in/s) (strain rate = 7.5×10^{-2} min^{-1}). Serrated grips with sandpaper covering the surfaces were used to grip the specimens. These specimens also had a gage length of 10.2 cm (4").

Molded specimen results are for a very limited number of specimens. No averaging of results was performed. All specimens fractured away from the grips and may be considered valid breaks.

RESULTS AND DISCUSSION

Materials

Figure 5 shows DSC curves for the pure polystyrene and the pure liquid crystal polymer. The PS exhibits a T_g at 104°C while the LCP exhibits a melt endotherm at 280°C. The LCP also shows two recrystallization peaks below the melt temperature. In DSC experiments up to 350°C no further peaks or transitions were observed for the LCP material.

Figure 6 shows rheological data for the two pure materials and the 40 w/0 blend at 285°C. Upper curves show shear stress as a function of shear rate while lower curves show viscosity. Fiber processing experiments were run at shear rates ranging from 100 to 10,000 s^{-1}. At $\dot{\gamma} = 100$ s^{-1}, the viscosity ratio (η_{LCP}/η_{PS}) is about 1.4 while at $\dot{\gamma} = 10{,}000$ s^{-1} the ratio increases to 4.0. The blend viscosity is slightly below that of either component at low shear rates and about equal to that of pure PS at higher shear rates. Low blend viscosity has been observed by many others who have examined LCP blends. For this reason, LCP's have been proposed as thermoplastic processing additives (17, 18).

Undrawn Fibers

Figure 7 shows fibrils from undrawn fibers after removing the PS matrix with toluene. At low (*Fig. 7c*) and high (*Fig. 7a,b*) shear rates, many irregular diameter fibrils are evident. At high shear rates, the fibrils are much finer and a variable diameter structure is prevalent—which, for lack of a better term, we label a stringbean structure. These stringbean structures appear to be in the process of necking down into finer fibrils. The regularity of the diame-

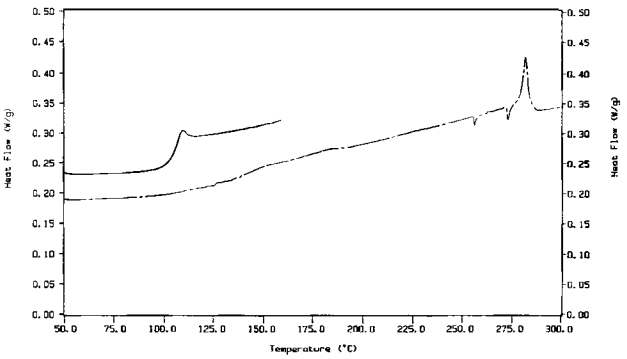

Fig. 5. DSC results for polystyrene and Vectra B-900. Polystyrene T_g at 103°C. LCP Tm at 280°C. Recrystallization peaks appear below LCP Tm.

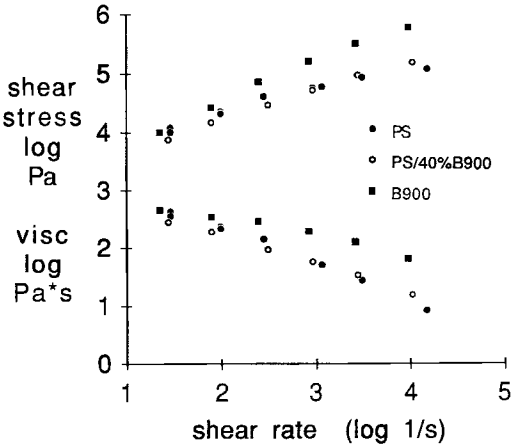

Fig. 6. Viscosity and shear stress vs. shear rate for polystyrene, Vectra B900 and a 40 w/0 LCP blend.

tral fluctuations suggests that perturbations in the flow might have caused the onset of the necking process. A stable neck forms between larger, unnecked sections of the fibril. At lower pressure at the entrance to the capillary, the fine stringbean structure is not as common (*Fig. 7c*); instead large fibrils of non-uniform diameters are prevalent.

Other authors have examined fibril formation in the converging die entrance and found droplet coalescence to occur there. Tsebrenko (1976), *et al.*, ran experiments in which the flow was quenched and the capillary was disassembled (6). Fibrils were found to coalesce in the entrance region of the capillary and a cross section with a "Vienna sausage" morphology was observed in the resulting fibrils. Our fibrils appear to have developed the same structure and then proceeded to neck down. Another interesting sign of coalescence can be seen in *7c* at the arrow, where a smaller fibril has apparently contacted a larger fibril and become attached, creating a Y in the fibrillar structure.

Transmitted light microscopy of the irregular fibrils shows a mottled texture within the fibrils (see *Fig. 7d*). This texture disappears as the fibril is drawn and the appearance becomes uniformly textureless. The texture may reflect the existence of crystalline grains which either become destroyed or aligned upon drawing. TEM examination may clarify this question and help to correlate it to the fracture behavior of the fibril, which is discussed below.

Fibril dispersion across the fiber is shown in the microtomed cross sections in *Fig. 8.* At the lower shear rates, fibrils tend to be rather large, with diameters from <1 μm to about 60 μm. At the high shear rates, fibrils are much smaller on average with a few larger fibrils up to 30 μm diameter but mostly small fibrils less than 1 μm in diameter.

Undrawn fiber fracture surfaces are shown in *Fig. 9. Figures 9a* and *9c* display the same fibril diameter

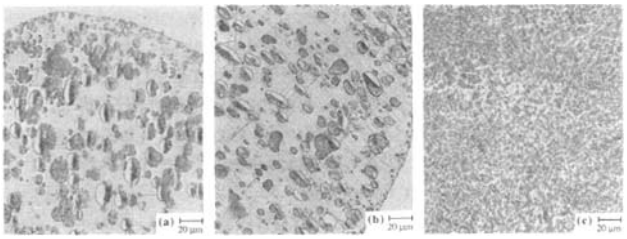

Fig. 8. Microtomed fiber cross sections at varying shear rates. All samples are undrawn. Dark regions are LCP (some LCP sections have folded back on themselves). (a) $\dot{\gamma}$ = 160 1/s. Fibril diameters range from 1 to 60 mm. (b) $\dot{\gamma}$ = 450 1/s. Fibril diameters range from 1 to 30 mm. (c) $\dot{\gamma}$ = 7630 1/s. Fibril diameters range from <1 to 20 mm.

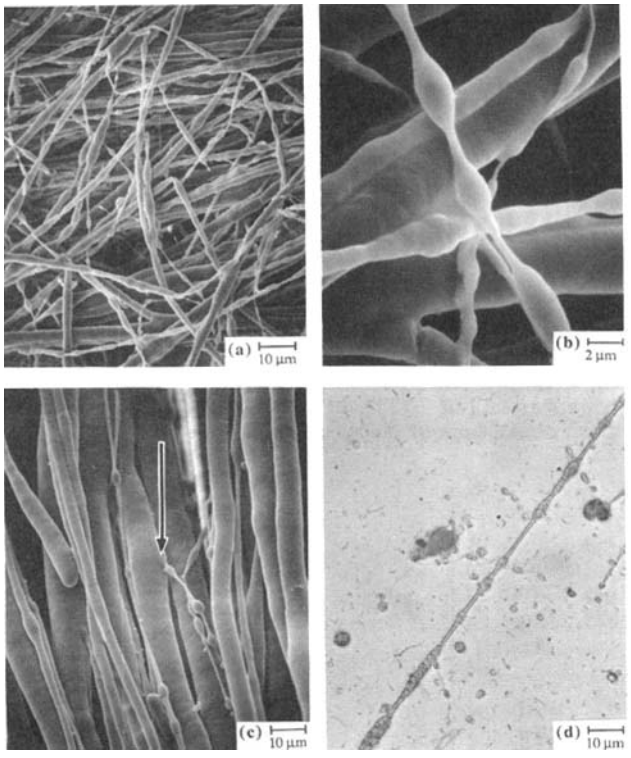

Fig. 7. Undrawn LCP fibrils after removal of polystyrene matrix with toluene. (a) $\dot{\gamma}$ = 7630 1/s. High shear rate produces fibrils with fluctuating diameters. (b) Detail from (a). (c) $\dot{\gamma}$ = 450 1/s. Low shear rate produces larger fibrils with moderate irregularity. Arrow points to junction of two fibrils—a sign of coalescence in the flow. (d) $\dot{\gamma}$ = 7500 1/s (approx.) Optical micrograph of high shear rate fibril. Undrawn regions exhibit a mottled texture while drawn regions appear textureless.

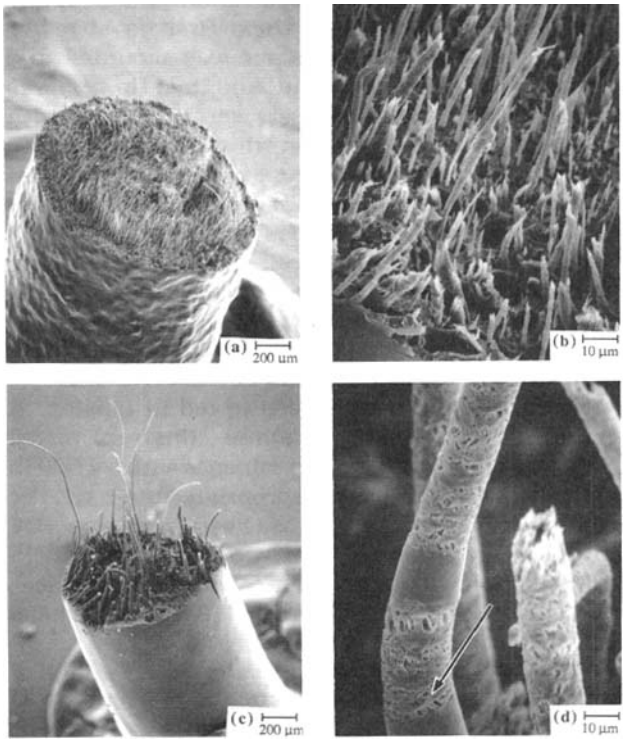

Fig. 9. Fracture surfaces of undrawn fibers. (a) $\dot{\gamma}$ = 6000 1/s. Note bumpy fiber exterior, obvious fibril pullout and flat fiber fracture surface indicating brittle polystyrene fracture. (b) $\dot{\gamma}$ = 6000 1/s. View of fracture surface showing torn fibril ends protruding from polystyrene matrix. (c) $\dot{\gamma}$ = 350 1/s. Low shear rate specimen. Smooth exterior shift of fiber. Larger fibrils exhibiting pullout. (d) $\dot{\gamma}$ = 160 1/s. View of fibril shaft showing twisting, opening tears resulting from tensile stress. Arrow points to well defined sigmoidal shaped openings.

variation with shear rate seen in *Figs. 7* and *8*; at low shear rates larger fibrils are seen, at higher shear rates many more fine fibrils are observed. In both samples the fracture surface shows considerable fibril-matrix debonding and pull-out. Poor interfacial adhesion is not surprising in light of the chemical dissimilarity between the non-polar polystyrene and the polar ester and amide groups of the LCP.

Closer examination of fibril structure after pullout at the fracture surface shows many broken fibrils with bands of irregular pores (*Figs. 9b* and *9d*). This occurs in the low and high shear rate samples. It appears that the tension applied in fracture has caused the fibril to twist and split, leaving sigmoidal-shaped openings (see arrow in *Fig. 9d*). The drawn fibrils do not fail in this manner, suggesting a correlation between the degree of molecular orientation, the mottled appearance (in optical microscopy), and the ability to fail by twisting and splitting. We speculate that molecular alignment may not be developed along the axis of the fibril in these undrawn samples and the lack of alignment contributes to the twisting and splitting failure. TEM and X-Ray examinations of the fibrils are planned to investigate this phenomenon.

The fiber made at low shear rates has a smooth exterior and those at high shear rates a bumpy texture. The latter is probably a result of melt instability which begins to occur at the higher extrusion pressure and shear rate.

Drawn Fibers

Figure 10a shows fibrils from a slightly drawn (d.r. = 2) fiber. The fibrils are more uniform in diameter than the undrawn fibrils, but considerable variation remains. The fibrils in *10c* were drawn to a d.r. = 7. These fibrils have attained a constant diameter. At higher draw ratios, the fibrils continue to draw, but the appearance does not change and the diameter remains uniform along the fibril.

Fibril diameter measurement is straightforward while fiber length determination is much more difficult. The finest fibrils we have observed have a diameter of approximately 0.15 μm. The undrawn microtome sections place a rough upper limit on fibril size at about 60 μm. In the drawn samples, the fibril are generally no larger than 15 μm for those obtained at low draw ratios and low shear rates, and considerably smaller for those at the higher shear rates—with maximum diameter around 6 μm and average diameter roughly 1 μm.

Attempts to follow a single fibril to its end were usually in vain. When single fibrils are extracted from a toluene dissolved specimen, the length is on the order of centimeters. This leads to estimates of length over diameter ratios which may range from a few hundred to more than 100,000. Other investigators have considered similar fibrils essentially infinite in length. It should be noted that, at the opposite extreme, small droplets of LCP which form in the extruder may not be elongated at all (see *Fig. 11*).

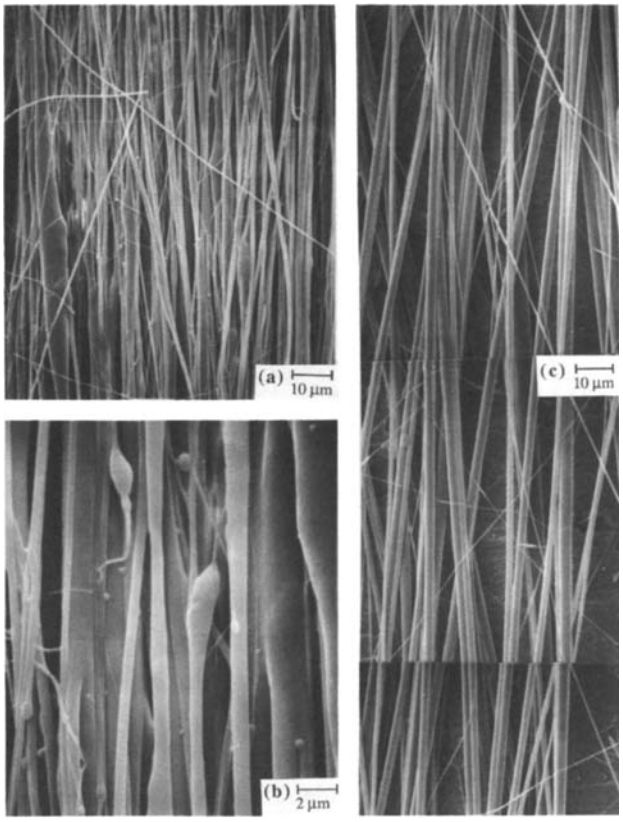

Fig. 10. Drawn LCP fibrils after removal of polystyrene matrix. (a) $\dot{\gamma}$ = 7630 1/s. draw ratio = 1.6. Fibrils are more regular than in undrawn material, but still exhibit irregular diameter. (b) $\dot{\gamma}$ = 7630 1/s. draw ratio = 1.6. Detail from (a). (c) $\dot{\gamma}$ = 450 1/s. draw ratio = 7. Fibril diameters are completely uniform. Fibrils are essentially infinite in length with no ends visible.

These droplets are small enough that elongational stresses cannot overcome interfacial tension and no elongation occurs.

Fracture surfaces of drawn fibers are shown in *Fig. 12*. The appearance is not changed appreciably by drawing. Because the LCP solidifies first in the cooling fiber, the fibrils cease drawing before the PS matrix. Evidence of this is seen in *Fig. 12C* where a distinct ridge on the surface of the fiber has formed over a fibril. This appears to indicate that the PS is drawn inward while the solidified fibril opposes the motion.

As mentioned above, the appearance of the fibrils at the fracture surface is substantially different in the drawn specimens. Whereas the undrawn fibrils sustain considerable damage to the fibril shaft, the drawn fibrils appear to suffer little damage below the fracture region (see *Fig. 12a*, *12b*).

Mechanical test results are given in *Figs. 13* and *14*. *Figure 13* shows modulus as a function of shear rate and draw ratio. The upper solid curve gives data for pure Vectra B900 published by Celanese (20). The lower solid curve is the value predicted for the blends by a rule-of-mixtures theory. Values for the higher-shear-rate samples fall quite near the rule-of-mixtures line. (The 1400 1/s samples were passed

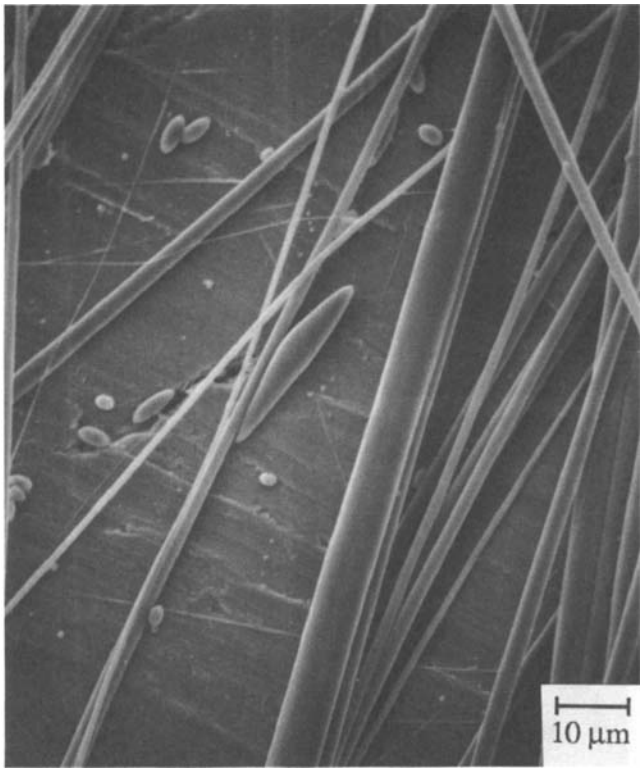

Fig. 11. Droplets from drawn LCP sample after removal of PS matrix. $\dot{\gamma}$ = 450 1/s, draw ratio = 7.

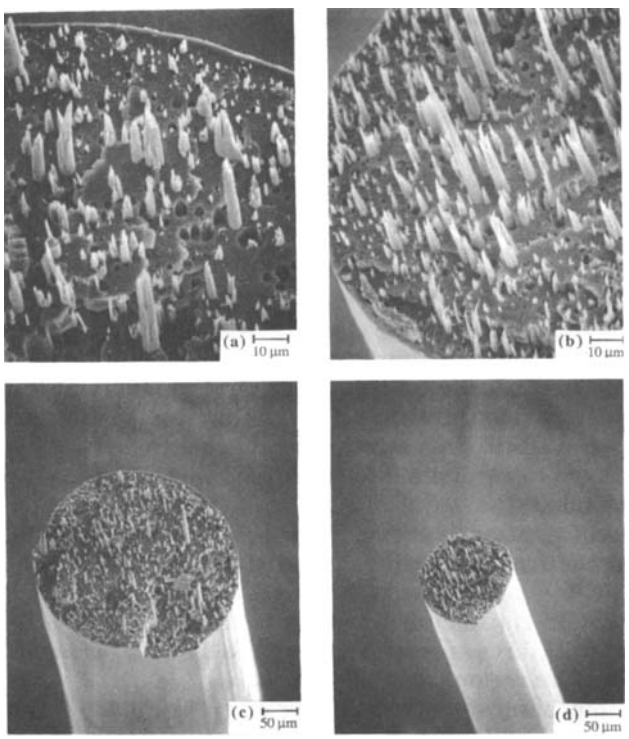

Fig. 12. Fracture surface of drawn fibers. $\dot{\gamma}$ = 450 1/s in all micrographs. (a) and (c) draw ratio = 7. (b) and (d) draw ratio = 30.

through the extruder at the higher shear rate [7630 1/s], but then the screw speed was reduced to lower pressure and extrudate velocity so that greater drawing could be performed with the drawing apparatus which was operating at its maximum drawing speed.) Values for the low-shear-rate samples fall substantially below the theory. Clearly the fine fibrils observed in the higher-shear-rate samples are contributing more to fiber reinforcement than the larger, low-shear-rate fibrils. X-Ray examinations are planned to determine the effects of shear rate on molecular orientation. The isolated x's on the graphs represent data for molded specimens which are discussed below.

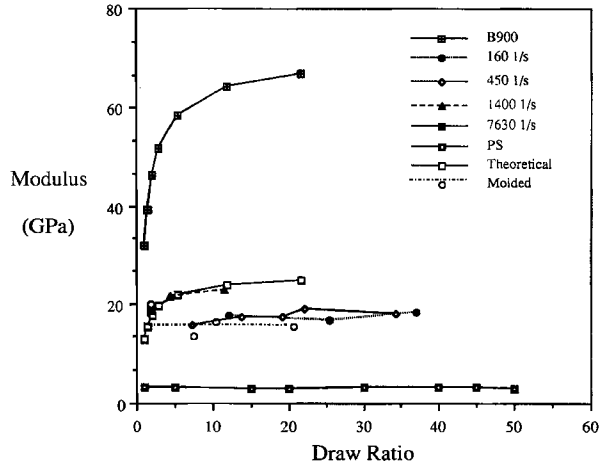

Fig. 13. Modulus vs. draw ratio for PS, B900 and blends extruded at various shear rates. B900 values derived from Celanese literature (20). Rule-of-mixtures curve calculated from theory assuming continuous, axially aligned fibrils. X's mark molded specimen data points.

Fiber strength data (*Fig. 14*) follow a similar pattern to stiffness data. Again the rule-of-mixtures line is drawn, though this prediction is more problematic than the modulus rule-of-mixtures prediction because strength depends on failure mode. The samples mixed at high shear rate and extruded at lower shear rate (1400 1/s) to allow drawing exhibit strength above the rule-of-mixtures prediction. Low-shear-rate samples fall below the theoretical strength. The strength of the highest-shear-rate samples also is below the rule-of-mixtures curve. It should be noted that all fibers were brittle in flexure—more so than either PS or B900. This suggests that many flaws—probably at the fibril ends—exist in the composite fibers.

Molded Specimens

Figure 15 shows a typical molded specimen fracture surface. The most obvious feature of this fracture surface is its similarity to the single-fiber fracture surface. Fibril pullout and a relatively flat polystyrene fracture surface are evident. The molding process can cause some movement of the fibrils. *Figure 16A* shows a polystyrene-rich region which has only a few of the finest fibrils. These fine fibrils were able to move with the polystyrene as it flowed. In *Fig. 16B* evidence of fibril misorientation is apparent. Although flow in the mold can cause fibril movement, the variation in this case is clearly the

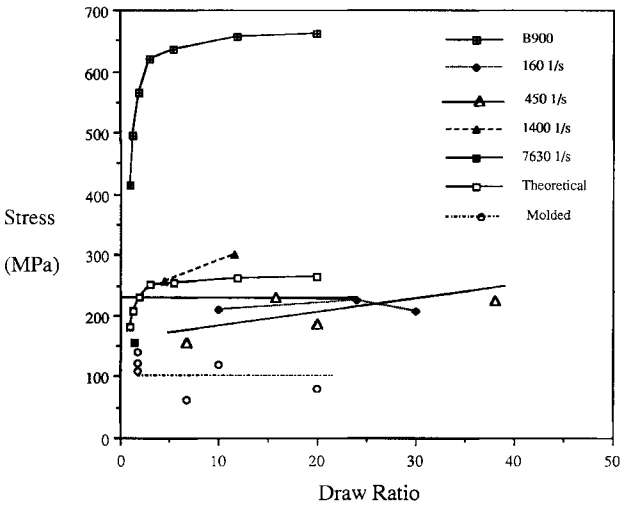

Fig. 14. Strength vs. draw ratio for B900 and blends extruded at various shear rates. B900 values derived from Celanese literature (20). Rule-of-mixtures curve calculated from theory assuming continuous, axially aligned fibrils. X's mark molded specimen data points.

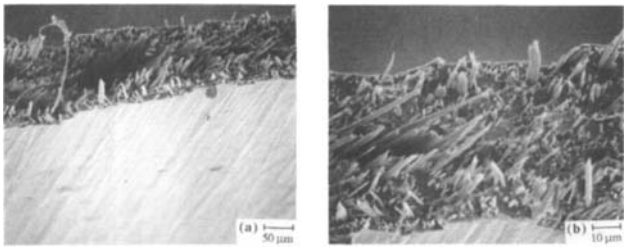

Fig. 15. Molded specimen fracture surface. Specimen molded from fibers extruded at $\dot{\gamma}$ = 450 1/s and draw ratio = 21.

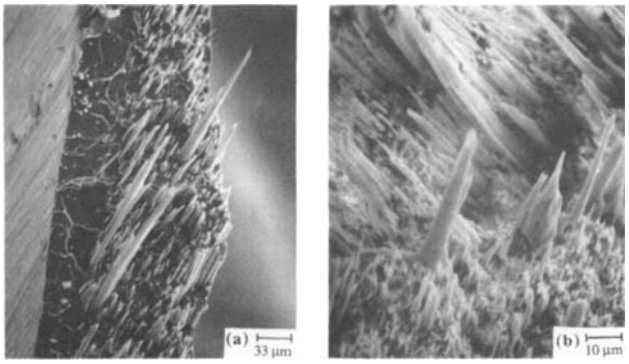

Fig. 16. Molded specimen fracture surfaces. a) Molded from fibers extruded at $\dot{\gamma}$ = 450 1/s and draw ratio = 21. Note polystyrene rich region at left with few fibrils. (b) Molded from fibers extruded at $\dot{\gamma}$ = 7630 1/s and draw ratio = 2. Note two regions with distinctly different fibril orientation resulting from fiber misalignment in mold.

result of original fiber misalignment, since two obvious groups of fibrils are evident.

Longitudinal modulus and strength of molded specimens are shown in *Figs. 13* and *14*. The moduli of the molded samples are represented by single points on the graphs. Because only a few molded specimens were made, the results must be interpreted with some caution. Data points represent single specimens rather than the average of several samples. The modulus of the molded specimens fell slightly below the modulus of the individual fibers. This result is predictable from the observation that some fibril misalignment occurs in the molded specimens.

Molded specimen strength was well below the fiber strength except in the case of the highest-shear-rate sample. Lower strength is expected from Weibull statistical considerations, which predict that strength will be a function of specimen size, with larger specimens having more flaws which can initiate the failure.

CONCLUSIONS

Production of composite structures by the proposed method is feasible. In this study we have successfully produced fibers containing reinforcing fibrils and molded those fibers into a composite structure reinforced by fibrils. The fibrils remain intact and essentially undisturbed by the molding process. In addition we have delineated processing conditions which lead to fibers and molded specimens which exhibit axial rule-of-mixtures stiffness and strength properties.

This work has perhaps raised many more questions than it has answered. These questions include:

1) What is occurring on the molecular level within the fibrils? The mottled-to-transparent texture transition and the variation in fibril failure appearance in the fractured specimens give clues, but more work is needed.

2) How much improvement in composite properties is possible by switching to a more compatible ductile matrix? Interfacial debonding in the PS/B900 system creates significant questions concerning the stress transfer from the elastic matrix to the stiff fibrils. In addition, a less brittle matrix material should show improved ultimate strength properties.

3) What improvements in properties is possible with different drawing conditions? For instance, a heated chamber could allow greater drawing of the LCP. A quench step after drawing may improve properties by lessening the relaxation of alignment attained in drawing.

4) The process developed here should be transferable to sheet extrusion. Ramanathan, Blizard, and Baird have performed film extrusion and drawing experiments. They report fibril formation in the extruded, drawn film (19).

ACKNOWLEDGMENTS

This research was supported by National Science Foundation Grant MSM8703791 and by a fellowship from the Macromolecular Science and Engineering Program. The materials were donated by Celanese Corp. and Dow Chemical Co. The assistance of Dr. F. Filisko at all stages of this research is also greatly appreciated. J. Huang, R. Pearson, and J. Covavisaruch contributed to specific aspects of the processing and analysis.

REFERENCES

1. G. I. Taylor, *Proc. Roy. Soc.*, **A146**, 501 (1934).
2. R. Cox, *J. Fluid Mech.*, **37**, 601 (1969).
3. F. Rumscheidt and S. Mason, *J. Colloid Sci.*, **16**, 238 (1961).
4. H. Van Oene, *J. Colloid Interface Sci.*, **40**, 3 (1972).
5. M. Tsebrenko, *Intern. J. Polym. Mater.*, **10**, 83 (1983).
6. M. Tsebrenko, A. V. Yudin, T. I. Ablazova, and G. V. Vinogradov, *Polymer*, **17**, 831 (1976).
7. A. Siegmann, A. Dagan, and S. Kenig, *Polymer*, **26**, 1325 (1985).
8. G. Kiss, *Polymer Eng. SPE Sci.*, **27**, 410 (1987).
9. K. Blizard and D. Baird, *SPE Antec '86 Prep.*, 311 (1986).
10. K. Blizard and D. Baird, *Polym. Eng. Sci.*, **27**, 653 (1987).
11. Y. Ide and Z. Ophir, *Polym. Eng. Sci.*, **23**, 261 (1983).
12. G. W. Calundann and M. Jaffe, *Proc. Robert A. Welch Conf. on Chemical Research XXVI*, Synthetic Polymers, 247 (1982).
13. G. Viola and D. Baird, *J. Rheol.*, **30**, 601 (1986).
14. A. Isayev and M. Modic, *SPE Antec '86 Prep.*, **573** (1986).
15. T. Chung, *SPE Antec '87 Prep.*, 1404 (1987).
16. M. Amano and K. Nakagawa, *Polymer*, **28**, 263 (1987).
17. N. Cogswell, U.S. Patent 4,433,083 (1984).
18. W. Huh, R. Weiss, and L. Nicolais, *Polym. Eng. Sci.*, **23**, 779 (1983).
19. R. Ramanathan, K. Blizard, and D. Baird, *SPE Antec '87 Prep.*, 1399 (1987).
20. *Extrusion of Celanese Vectra Resins*, an otherwise unlabeled brochure supplied by Celanese.